HHS Public Access

Author manuscript

ACS Infect Dis. Author manuscript; available in PMC 2018 May 16.

Published in final edited form as:

ACS Infect Dis. 2017 August 11; 3(8): 606–619. doi:10.1021/acsinfecdis.7b00065.

Investigating the interaction of octapeptin A3 with model bacterial membranes

Mei-Ling Han[1,2], **Hsin-Hui Shen**[3,*], **Karl A. Hansford**[4], **Elena. K. Schneider**[2], **Sivashangarie Sivanesan**[2], **Kade**, **D. Roberts**[2], **Philip E. Thompson**[2], **Anton P. Le Brun**[5], **Yan Zhu**[1,2], **Marc-Antoine Sani**[6], **Frances Separovic**[6], **Mark A.T. Blaskovich**[4], **Mark A. Baker**[7], **Samuel M. Moskowitz**[8], **Matthew A. Cooper**[4], **Jian Li**[1], and **Tony Velkov**[2,*]

[1]Monash Biomedicine Discovery Institute, Department of Microbiology, Monash University, Clayton, Victoria 3800, Australia

[2]Drug Development and Innovation, Drug Delivery, Disposition and Dynamics. Monash Institute of Pharmaceutical Sciences, Monash University, 381 Royal Parade, Parkville 3052, Victoria, Australia

[3]Department of Materials Science and Engineering, Faculty of Engineering, Monash University, Clayton, Victoria 3800, Australia

[4]Institute for Molecular Bioscience, The University of Queensland, Brisbane, Queensland 4072, Australia

[5]Bragg Institute, Australian Nuclear Science and Technology Organisation, Locked Bag 2001, Kirrawee DC, New South Wales 2232, Australia

[6]School of Chemistry, Bio21 Institute, University of Melbourne, VIC 3010, Australia

[7]Priority Research Centre in Reproductive Science, School of Environmental and Life Sciences, University of Newcastle, Callaghan, NSW, 2308, Australia

[8]Vertex Pharmaceuticals, Boston, MA, United States

Abstract

Octapeptins are cyclic lipopeptides that do not exhibit cross-resistance with polymyxins and have a broader spectrum of activity that includes fungi and Gram-positive bacteria. In the present study we investigated the interaction of octapeptin A3 with asymmetric outer membrane models of the Gram-negative pathogen *Pseudomonas aeruginosa*, using neutron reflectometry, together with fluorimetric and calorimetry methods. For the first time our neutron reflectometry results reveal that the interaction of octapeptin A3 with the Gram-negative outer membrane involves an initial transient polar interaction with the phospholipid and lipid A head groups, followed by the penetration of the entire octapeptin molecule into the fatty acyl core of the outer membrane. This mechanism contrasts that of polymyxin B which specifically targets lipid A, whereas octapeptins

[*]Corresponding authors, Address correspondence to: Tony.Velkov@monash.edu or Hsinhui.Shen@monash.edu or colistin.polymyxin@gmail.com; Correspondence: Tony Velkov, Phone: +61 3 9903 9539. Fax: +61 3 9903 9583. Tony.Velkov@monash.edu; *Joint senior authors.

Associated content: Supporting Information. The Supporting Information is available free of charge on the ACS Publications website.

appear to target both lipid A and phospholipids. Furthermore, the mechanism of octapeptins does not appear to be highly dependent on an initial complimentary electrostatic interaction with lipid A, which accounts for their ability to bind to the lipid A of polymyxin-resistant Gram-negative bacteria which is modified with cationic moieties that act to electrostatically repel the cationic polymyxin molecule. The presented findings shed new light on the mechanism whereby octapeptins penetrate the outer membrane of polymyxin-resistant Gram-negative pathogens and highlight their potential as candidates for development as new antibiotics against problematic multi-drug resistant pathogens.

Graphical abstract

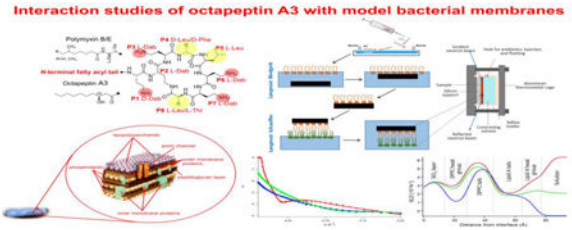

Introduction

The decline in the discovery and development of novel antibiotics, combined with in the emergence of bacteria resistant to almost all available antibiotics is of grave concern. Currently, polymyxin B and E (colistin) are being used as the last-line therapy against life-threatening Gram-negative infections, unfortunately resistance to polymyxins in both the community and hospital setting is becoming more common.[1-2] Octapeptins are structurally related non-ribosomal lipopeptide antibiotics that do not exhibit cross-resistance with polymyxins and have a broader spectrum of activity that includes fungi and Gram-positive bacteria. This makes them a precious and finite resource for the development of new antibiotics against these problematic polymyxin-resistant Gram-negative pathogens, in particular *Pseudomonas aeruginosa*, *Acinetobacter baumannii* and *Klebsiella pneumoniae*.

The ocatapeptins were discovered over three decades ago as natural products of the soil bacteria *Bacillus circulans*.[3-7] Originally, the name ‘octapeptins’ was given to a group of lipopeptide antibiotics discovered in the 1970s which were given the company compound codes Bu-2470, EM49, 333-25 and Bu-1880 by two independent groups from what were at the time the Squibbs and Bristol-Myers pharmaceutical development laboratories.[3-11] Eventually a consensus on nomenclature was reached and these octatpeptins were alphabetically designated into four sub-groups A, B, C, D based on minor structural differences in their core scaffold.[8] Structurally, the octapeptins can be considered as a sub-class of cyclic lipopeptides which have a truncated exocyclic linear peptide segment and smaller cyclic peptide segment. Fundamentally, the polymyxins are cyclic decapeptides whereas the ocatapeptins, as per their namesake are cyclic octapeptides. Similarities include the presence of cationic Dab residues at positions 1-3 and 6 & 7, also residues 1-4 in the octapeptins correspond to positions 3-6 in the polymyxin B sequence (Figure 1).

There has been a marked resurgence of interest in the re-development of ‘old’ antibiotics. Not unlike the polymyxins, interest in the development of the octapeptins as therapeutics waned as the β-lactam antibiotics were favoured at the time due to their low toxicity and ideal pharmacological profiles. As a consequence, the literature and pharmaceutical development sector has been essentially devoid of octatpeptin research for the past 30 years. Very little is known about the primary mode of action of octapeptins apart from the fact that they bind and insert into phospholipid layers, perturbing the outer membrane structure, which helps explain their broad antimicrobial activity.[12] Since octapeptins are amphipathic in character (Figure 1), at first glance it may be assumed that their disruptive influence on the bacterial outer membrane may be attributed to an activity akin to that of a simple cationic detergent. However, this is not the case as octapeptins exhibit bactericidal activity at much lower concentrations than simple cationic detergents and, moreover, they display dose-dependent activity.[5, 9, 13] Furthermore, minor structural modifications to the octapeptin core scaffold can produce significant changes in their bactericidal activity.[8, 12] Taken together, these findings highlight that specific interactions between the octapeptin molecule and the bacterial membranes are at play. Understanding the interactions of octapeptins with the Gram-negative outer membrane (OM) of polymyxin resistant strains is fundamental for advancing the development of octapeptins as next-generation lipopeptide antibiotics against these problematic human pathogens. This study employed neutron reflectometry (NR), together with fluorimetric and calorimetry techniques to investigate the interaction of octapeptin A3 with asymmetric membrane models of the *P. aeruginosa* OM. These novel findings shed light on a unique mechanism whereby octapeptins penetrate the OM of polymyxin-resistant Gram-negative pathogens.

Results and Discussion

Total synthesis and antibacterial activity of octapeptin A3

We report the first synthesis of octapeptin A3 in 21% overall yield (Figure 1) using Fmoc-based solid-phase peptide synthesis methodology (*cf.* Experimental Section). Antimicrobial activity was screened against a panel of ATCC and clinical isolates of polymyxin-susceptible and -resistant strains of *P. aeruginosa, A. baumannii* and *K. pneumoniae, E. cloacae* and Gram-positive *Enterococcus faecium* and *Staphylococcus aureus*; polymyxin B and colistin were used as comparators (Table S1). Octapeptin A3 showed moderate activity (minimum inhibitory concentrations, MICs 4 - 32 mg/L) against the polymyxin-susceptible strains of *K. pneumoniae, A. baumannii* and *E. cloacae*, with comparatively lower activity to both polymyxin B and colistin (MICs 0.5-8 mg/L). Similar to polymyxin B and colistin, octapeptin A3 displayed poor activity against the Gram-positive methicillin-resistant *S. aureus*, and *E. faecium* (MIC 32 mg/L); and moderate activity against the polymyxin-resistant strains of *K. pneumoniae* and *A. baumanii* (MICs 8-32 mg/L). Octapeptin A3 was most active against *P. aeruginosa*: against the polymyxin-susceptible strain *P. aeruginosa* ATCC 27853 octapeptin A3 showed comparable activity (MIC 2 mg/L) to that of polymyxin B and colistin (MIC 1 mg/L); whereas, against the polymyxin-resistant (MICs 4-128 mg/L) strains of *P. aeruginosa*, octapeptin A3 displayed superior activity (MICs 1-2 mg/L).

In light of the superior antimicrobial activity of octapeptin A3 against a polymyxin-susceptible and -resistant strain of *P. aeruginosa*, static time-kill studies were performed to evaluate the antimicrobial kinetics (Figure S1), colistin was employed as the comparator. For the polymyxin susceptible strain of *P. aeruginosa* ATCC 27853 (colistin MIC 1 mg/L; octapeptin A3 MIC 2 mg/L), both colisitin and octapeptin A3 displayed comparable killing kinetics, with a >2 $\log_{10}$ reduction in colony-forming units CFU/mL units over 1-6 h at ×2-4 MIC (Figure S1). However, under all concentrations of octapeptin A3 or colistin substantial regrowth occurred at 24 h, suggesting the development of resistance. In the polymyxin-resistant *P. aeruginosa* strain 19147R (colistin MIC >128 mg/L; octapeptin A3 MIC 1 mg/L) colistin showed no bacterial killing effect. Whereas at ×1-4 MIC, octapeptin A3 displayed slower killing kinetics with a ~4 $\log_{10}$ reduction in CFU/mL units, with no bacterial growth detectable between 4-6 h at ×2 and ×4 MIC. Notwithstanding, substantial regrowth was still evident at 24 h under all treatment conditions.

The *in vivo* activity of octapeptin A3 was accessed in mouse bacteremia *P. aeruginosa* infection model. In the *P. aeruginosa* ATCC 27853 (polymyxin B MIC 0.5 mg/L; octapeptin A3 MIC 2 mg/L) bacteremia infection model, intravenous dosing of octapeptin A3 (dose 4 mg/kg) had a moderate effect (-1.22 log-fold reduction) on the bacterial load compared to the untreated control mice after 4 h; whereas polymyxin B (dose 4 mg/kg) produced a -2.55 log-fold reduction in the bacterial load. Against the polymyxin-resistant strains *P. aeruginosa* 18878B (polymyxin B MIC >32 mg/L; octapeptin A3 MIC 1 mg/L) and 19147n/m (polymyxin B MIC >32 mg/L; octapeptin A3 MIC 2 mg/L) octapeptin A3 (dose 4 mg/kg) displayed a similar level of activity producing a log-fold reduction in the bacterial load at 4 h of -1.11 and -1.38, respectively. In contrast, polymyxin B (dose 4 mg/kg) displayed no effect or very poor activity (*P. aeruginosa* 18878B -0.37 log-fold reduction; *P. aeruginosa* 19147n/m 0.05 log-fold reduction). Overall, these findings suggest that octapeptin A3 displays potent and selective anti-pseudomonal activity against polymyxin resistant strains.

Isolation and structure determination of lipid A from the stable polymyxin-resistant P. aeruginosa strain PAKpmrB6

Structures of lipid A isolated from the polymyxin-resistant strain *P. aeruginosa* PAK*pmrB6* were elucidated through LC/MS/MS, which displayed major peaks at *m/z* 1895.10, 1879.11, 1724.97, and 1707.97, corresponding to the addition of two 4-amino-4-deoxy-L-arabinose (L-Ara4N) moieties to the phosphates of the wild-type lipid structure which is represented by peaks at *m/z* 1632.99, 1615.99, 1461.85, and 1445.86, respectively (Figure 2). The peaks at *m/z* 1764.05, 1748.05, 1592.91, and 1576.92 correspond to the lipid A structure with the addition of a single L-Ara4N group. Other major peaks at *m/z* 1684.08, 1667.08, 1512.94, and 1496.95 correspond to the degradation of a phosphate group ($\Delta m/z = -80$) from the structures listed above. Our data was consistent with previously reported results.[14] In addition, the percentage of each lipid A species which was used to calculate the scattering length density (SLD) of Ara4N-lipid A applied in NR study was obtained from LC-MS analysis, apparently, penta-acylated lipid A modified with one L-Ara4N (peaks at *m/z* 1512.94, and 1496.95) is the predominant constituent (Table S2).

Interaction of polymyxin B with Ara4N-lipid A:d62-DPPC bilayer investigated by neutron reflectometry

NR is a state-of-the-art technology which can (1) characterise the structure of biological membranes, (2) resolve the structure of peptides in the membrane, and (3) provide nanometer-resolution spatial information on the membrane components.[15] With the high penetration depth of neutrons, NR is the only platform that is able to reveal high-resolution and quantitative mechanistic information for peptides interacting with a biological membrane in a non-destructive manner.[16] NR was conducted to study the interactions between lipopeptides and Gram-negative outer membrane (OM) model. The OM model was constructed through sequential Langmuir-Blodgett and Langmuir-Schaefer deposition methods (Figure S5).[17-19] L-Ara4N modified lipid A isolated from PAK*pmrB6* was used to form the outer leaflet of OM, and the inner leaflet of OM was formed by 1, 2-dipalmitoyl(d62)-sn-glycero-3-phosphocholine (d62-DPPC).The NR profiles obtained from the Ara4N-lipid A:d62-DPPC bilayer were fitted to a minimal six-layer model to describe the interfacial structure, i.e. sequentially from silicon to solution, a hydrated silicon oxide layer, the d62-DPPC head groups, the d62-DPPC tails, the lipid A tails, the lipid A glucosamine (GlcN) head groups, and the lipid A L-Ara4N head groups (Figure 3A). Analysis of the bilayer by NR revealed that an asymmetric lipid composition had been deposited on the silicon-water interface with an inner layer composed of 83% d62-DPPC and 13.5% of lipid A, and an outer layer composed of 76.8% lipid A and 20.4% of d62-DPPC; 3.5% and 2.8% water were found in inner and outer layer, respectively. The inner head groups (d62-DPPC) and outer head groups (lipid A GlcN) displayed a water composition of 10.2% and 8.7%, respectively. An extra layer was fitted for the lipid A Ara4N head groups, representing a thickness as 9.0 Å and composition of 64.8% Ara4N and 35.2% water (Table 1).

The NR signal slightly decreased after polymyxin B injection onto the bilayer surface at 4 mg/L (Figure 3B). NR analysis indicated a polymyxin B layer with volume fraction of 21.7 ± 1.3% and thickness of 10.0 Å bound to the surface of the Ara4N-lipid A:d62-DPPC bilayer (Table 1; Figure S2 and Table S3), albeit, no significant changes to the coverage or asymmetry of the Ara4N-lipid A:d62-DPPC bilayer were observed (Table 1). This result suggests polymyxin B only binds to the surface of the Ara4N-lipid A:d62-DPPC bilayer and does not penetrate into the lipid A head group or fatty acyl regions.

Interaction of octapeptin A3 with Ara4N-lipid A:d62-DPPC bilayer investigated by neutron reflectometry

In preparation for the octapeptin A3 interaction studies, the Ara4N-lipid A:DPPC bilayer was reproduced (Figure 4A and Table 2). Specifically, the Ara4N-lipid A: DPPC bilayer was composed of 73.5% d62-DPPC and 21.6% lipid A in the inner leaflet, whereas a nearly converse composition of 67.4% lipid A and 26.5% d62-DPPC was observed in the outer leaflet of the bilayer. A similar proportion of water, 4.9 and 6.1% were found between inner and outer layer, respectively. The inner head groups (d62-DPPC) and outer head groups (lipid A GlcN) displayed a water composition of 11.4% and 12.9%, respectively. The lipid A Ara4N head group was fitted to a thickness of 8.5±0.5 Å and found to be composed of 44.8 % Ara4N and 55.2% water (Table 2). The injection of octapeptin A3 at a concentration

of 1 mg/L onto the bilayer surface led to a dramatic shift in the NR profile (Figure 4B). NR analysis indicated a octapeptin A3 layer with volume fraction of 16.1 ± 0.5% and thickness of 9.6 Å bound to the surface of the Ara4N-lipid A:d62-DPPC bilayer (Table 3; Figure S3 and Table S4). Approximately, 9.3 ± 1.4% and 5.5 ± 2.0% octapeptin A3 was observed penetrating the lipid A Ara4N and GlcN head groups, respectively. In contrast to polymyxin B which showed no penetration, a significant volume fraction of octapeptin A3 was observed in the DPPC and lipid A tail regions (17.3 ± 1.6% and 25.8 ± 2.5%, respectively). In addition, a further decrease in NR profile of the Ara4N-lipid A: DPPC bilayer was observed following the injection of a higher concentration of octapeptin A3 (4 mg/L) (Figure S4). Notably, a greater volume fraction of octapeptin A3 (22.2 ± 0.8%) binding to the surface of the Ara4N-lipid A:DPPC bilayer was observed compared to the lower octapeptin A3 concentration (1 mg/L). Interestingly, penetration into the bilayer was comparable at both the low and high octapeptin A3 concentrations (Table S5). These NR results suggest that, unlike polymyxin B which did not penetrate the Ara4N-lipid A:DPPC bilayer and sits on the surface, the octapeptin A3 is capable of penetrating deep into the DPPC and Ara4N-lipid A tail regions of the bilayer.

Binding of octapeptin A3 to P. aeruginosa LPS evaluated by Isothermal Titration Calorimetry

Microcalorimetric measurements of octapeptin A3 binding to *P. aeruginosa* LPS yields the total heat signal from each injection over time (Figure 5). The area under the individual peaks was determined and plotted *vs.* the [octapeptin A3]/[LPS] molar ratio. The heat of dilution data were analyzed to determine the association constant (K_D), number of binding sites (n), the entropy (ΔS) and enthalpy of binding (ΔH) (Table S6). Titration curves corresponding to an exothermic reaction were observed for both colistin and octapeptin A3. The thermodynamic parameters for the interaction of octapeptin A3 at 37°C revealed an approximately 3:1 [octapeptin A3:LPS] binding stoichiometry with a moderate binding affinity (K_D=1.6 μM). In comparison, the thermodynamic parameters for the interaction of colistin at 37°C revealed an approximately 1.5:1 [colistin: LPS] binding stoichiometry with a low-to-moderate binding affinity (K_D=5.6 μM). The binding of octapeptin A3 to *P. aeruginosa* LPS was largely driven by a favourable (negative) enthalpic component and displayed an unfavourable entropic (negative) component. In comparison the binding of colistin to *P. aeruginosa* LPS was largely driven by a favourable (negative) enthalpic component and a favourable entropic (positive) component. Taken together these parameters suggest that complexation of both lipopeptides with *P. aeruginosa* LPS is driven by a combination of ionic and hydrophobic interactions.

Displacement of the dansyl-polymyxin probe FADDI-043 from P. aeruginosa LPS

The ability of octapeptin A3 to compete with the dansyl-polymyxin probe FADDI-043 (aka MIPS-9541) for binding to *P. aeruginosa* LPS was examined fluorimetrically (Figure 6).[20-22] The concentration of octapeptin A3 or the comparator colistin required to achieve 50% displacement (I_{50}) was used to calculate K_i values as a measure of the LPS binding affinity of the displacing lipopeptide. In line with the ITC results, the fluorescence displacement assay revealed octapeptin A3 (K_i=0.85±0.15 μM) displayed higher affinity for *P. aeruginosa* LPS compared with colistin (K_i=1.32±0.03 μM).

Large unilamellar vesicle (LUV) dye release

LUV dye-release experiments measure the ability to permeabilise the LUV membrane as reflected as the extent of fluorescent dye leakage over time following lipopeptide exposure.[23] The detergent, Triton X-100, was used a positive control and added at 1700 sec to completely lyse the LUVs, producing a maximum fluorescence response. The dye release experiments revealed that colistin produced a concentration-dependent dye release profile with both the LPS-free and LPS loaded LUVs (Figure 7). Notably, colistin produced a higher level of dye release with the *P. aeruginosa* LPS-loaded LUVs. By comparison, octapeptin A3 produced a concentration-independent dye release in the LPS-free LUVs and no dye release in the LPS-loaded LUVs.

Conclusions

Octapeptins are cyclic lipopeptides that exhibit a broad spectrum of activity against polymyxin-resistant microorganisms. Our biophysical studies revealed that this extended activity involves a mode of action wherein the octapeptin molecule interacts with lipid A and phospholipid head groups through polar contacts, and subsequently the entire octapeptin molecule penetrates deeper into the fatty acyl tail region of the Gram-negative OM bilayer. This is in contrast to the mechanism of polymyxins against Gram-negatives where the initial OM binding event is highly dependent upon complementary electrostatic interactions between the cationic Dab side chains of the polymyxin molecule and the anionic phosphates of lipid A. This electrostatic event is then followed by stabilizing hydrophobic contacts between the lipid A fatty acyl chains and the *N*-terminal fatty acyl and position 6 & 7 hydrophobic motifs of the polymyxin molecule. Importantly, our results highlight that, unlike polymyxins which specifically target lipid A, octapeptin A3 is capable of binding to both phospholipids and LPS, independently. Taken together, this may account for the ability of octapeptins to attack the cytoplasmic membrane of Gram-positive bacteria and fungi, which lack LPS and are predominately composed of phospholipids. Furthermore, the finding that octapeptins are not highly dependent on complementary electrostatic interactions accounts for their activity against polymyxin-resistant Gram-negative bacteria that express lipid A modified with cationic moieties that serve to repel the polymyxin molecule. Notwithstanding, the precise mode of action of octapeptins remains unclear and their target(s) maybe multiple, i.e. OM, periplasmic or intracellular, and importantly how this unique antimicrobial activity relates to their structure toxicity relationships. Overall, our findings highlight that the octapeptins are a class of lipopeptides with a novel mode of action, broad antimicrobial activity and unique physicochemical properties that underscore their potential for development as antibiotics.

Experimental Section

Materials

All chemicals were purchased from Sigma-Aldrich at the highest research grade. Ultrapure water was from Fluka (Castle Hill, Australia). All phospholipids were purchased from Avanti Polar Lipids, >99% purity (Alabaster, AL) and used without further purification.

Stock solutions of octapeptin A3 (10 mg/L) were prepared in Milli-Q™ water (Millipore, Australia) and filtered through 0.22 μm syringe filters (Sartorius, Australia).

Octapeptin A3 lipopeptide synthesis

General Experimental—LC-MS analyses were conducted using a Shimadzu LCMS 2020 or Agilent Technologies 1200 Series Instrument. Compounds were purified by MPLC (Grace Reveleris X2) or by HPLC (Agilent Preparative HPLC 1260 Infinity Series). *Eluent 1*: 0.05% formic acid in water (A) and 0.05% formic acid in acetonitrile (B). *Eluent 2*: 0.05% trifluoroacetic acid (TFA) in water (A) and 0.05% TFA in acetonitrile (B). *Eluent 3*: water (A) and acetonitrile (B). HPLC columns – *Column 1*: Agilent Eclipse XDB phenyl; 4.6 × 150 mm, 5 μ. *Column 2*: Agilent Eclipse XDB phenyl; 30 × 100 mm, 5 μ. *Column 3*: Grace Reverleris C18 RP 12g cartridge. HPLC methods – *Method 1*: eluent 1, column 1, flow 1 mL/min. Ratios refer to solvents A & B, respectively: 95:5, 0.5 min; 95:5 to 0:100, 8.5 min; 0:100, 2 min. *Method 2*: eluent 3, column 3, flow 30 mL/min. Ratios refer to solvents A & B, respectively: 100:0, 1.3 min; 100:0 to 0:100, 6.4 min; 0:100, 2.3 min. *Method 3*: eluent 2, column 2, flow 20 mL/min. Ratios refer to solvents A & B, respectively: 95:5 to 47.5:52.5, 10 min. The MS/MS spectra were obtained using an API QSTAR™ Pulsar Hybrid LC-MS/MS System. High resolution mass spectrometry (HRMS) was performed on a Bruker Micro TOF mass spectrometer using (+)-ESI calibrated to NH_4OAc.

Materials—H-L-Leu-2-chlorotrityl resin, O-(1H-6-Chlorobenzotriazole-1-yl)-1,1,3,3-tetramethyluronium hexafluorophosphate (HCTU), Fmoc-L-Dab(ivDde)-OH, Fmoc-L-Dab(Boc)-OH, Fmoc-D-Dab(Boc)-OH, Fmoc-L-Leu-OH and 1,1,1,3,3,3-hexafluoroisopropyl alcohol (HFIP) were purchased from Chem-Impex International Inc. (Wood Dale, IL). 3-(*R*)-Hydroxydecanoic acid methyl ester was purchased from Toronto Research Chemicals, Inc. (Toronto, Canada).

3-(*R*)-Hydroxydecanoic acid—3-(*R*)-hydroxydecanoic acid methyl ester, (3.97 g, 19.6 mmol) in tetrahydrofuran (THF, 35 mL) was treated dropwise with a solution of $LiOH.H_2O$ (2.42 g, 57.7 mmol) in H_2O (35 mL) at ambient temperature. After stirring overnight, the mixture was acidified with 1M HCl to pH 2-3. The solution was extracted with EtOAc (4 × 50 mL). The pooled organic phase was dried ($MgSO_4$), filtered and evaporated *in vacuo* to give 3-(*R*)-hydroxydecanoic acid as a colourless solid which was used without further purification. Yield: (3.48 g, 94% yield).

1. Synthesis of Octapeptin A3

1.1 Solid phase synthesis: resin 1a

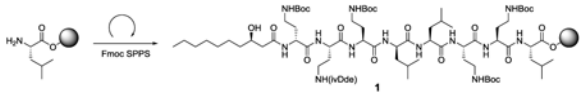

The starting resin H-L-Leu-2CT (303 mg, 0.201 mmol, 0.67 mmol/g) was pre-swollen in THF and then briefly washed with DCM (× 3) and DMF (×3). The appropriate Fmoc-amino acid (2 equiv.) was dissolved in a solution of HCTU (0.281 M, 2.1 equiv.), treated with DIPEA (4 equiv.), and allowed to stand for 5 min. The pre-activated amino acid solution was

added to the resin. After shaking for 2 h, the solvent was drained and the resin was washed with DMF (× 3).

Coupling efficiency was monitored by treatment of a small quantity of resin (1-3 mg) with 95:2.5:2.5 TFA/triisopropyl silane/H_2O (10 μL) for 15 min, followed by suspension in 1:1 acetonitrile/H_2O (1 mL), filtration and LC/MS analysis. In this manner, all couplings were deemed quantitative at each step. The Kaiser test was prone to false positives and was not a reliable indicator of coupling efficiency.

Fmoc deprotection was effected by two successive treatments of the resin with piperidine in DMF (30:70, *ca.* 10 mL per gram of resin) at ambient temperature (1 × 10 min, 1 × 20 min). The solvent was drained and the resin was washed with DMF (× 3) between each treatment, and following completion of the sequence.

Peptide synthesis was completed by acylation of the *N*-terminus with 3-(*R*)-hydroxydecanoic acid (1.5 equiv.) using the same protocol outlined above. The resin was washed with DMF (× 3), DCM (× 3), IPA (× 3), DCM (× 3), IPA(× 3), and then dried under vacuum overnight. The final weight of the resin 1 was 551 mg (91% of theoretical).

1.2 ivDde removal from resin 1

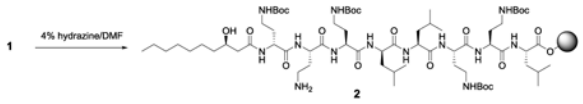

Resin 1 (551 mg) was pre-swollen in DCM for 10 min. The solvent was drained and the resin was treated with a solution of 4% hydrazine hydrate in DMF (2 mL, *ca.* 9 equiv.) for 1 h at ambient temperature. The solvent was drained, and the resin was washed with DMF (× 3). The process was repeated (1 mL hydrazine solution, *ca.* 4.5 equiv.), after which the resin was successively washed with DMF (× 3), THF (× 3), IPA (× 3), DCM (× 3) and IPA (× 3). The resulting deprotected resin **2** was dried under vacuum overnight. The final weight of the resin was 500 mg (89% of theoretical).

1.3 Resin cleavage: compound 2

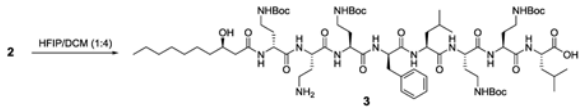

Resin 2 (500 mg, 0.359 mmol/g, 0.18 mmol) was treated with a solution of HFIP in DCM (1:4, 15 mL) for 90 min. The solvent was drained and the resin was washed with DCM (× 3). The filtrates were pooled, evaporated and then dried under vacuum overnight to afford crude **3** (0.269 g, 105% of theoretical) as a cream solid. t_R 6.7 (Method 1). (ES) m/z 1428.8 (MH^+). The material was used without further purification.

1.4 Off-resin cyclisation of linear precursor 3

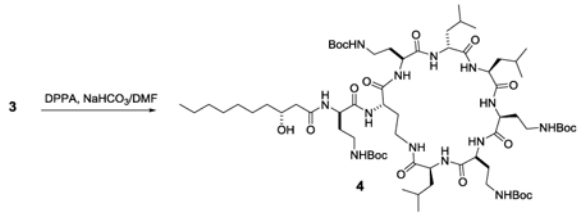

Crude **3** (0.269 g, assume 0.18 mmol) was dissolved in DMF (22 mL, 0.008 M), and treated with $NaHCO_3$ (300 mg, *ca.* 20 equiv.) followed by DPPA (76 μL, 0.36 mmol, 2 equiv.). The mixture was stirred at ambient temperature overnight. The reaction was monitored by LC/MS analysis (method 1; t_R 6.7 linear, t_R 7.54 cyclised). The mixture was filtered through a bed of Celite, and the solvent was evaporated. Traces of DMF were removed by co-evaporation from heptane (× 3), and the resulting product was dried overnight under vacuum to afford crude cyclised product **2c** (444 mg). The crude solid was suspended in excess pentane and stirred overnight to produce a uniform off-white solid that was collected by filtration. The cake was washed with pentane and the solid was dried under vacuum overnight to afford the crude cyclised product **4**, a cream powder (312 mg). Crude **4** was purified by RP-HPLC (Method 2). The final yield of the fully protected octapeptin-A3 precursor **4** was 130 mg (51% yield, >97% purity). t_R 7.5 (Method 1). (ES) m/z 1410.8 (MH^+), 1311.4 2 (MH^+-Boc).

1.5 Octapeptin A3: final deprotection and purification

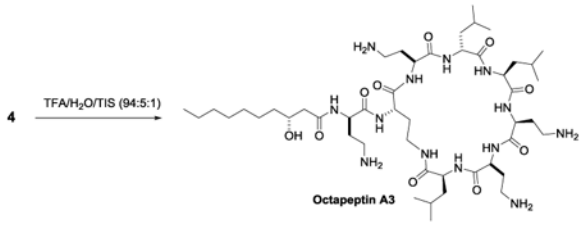

Purified **4** (130 mg, 0.092 mmol) was dissolved in 94:5:1 TFA/H_2O/TIS (7 mL) and allowed to stand at ambient temperature for 30 min. Volatiles were removed under reduced pressure and the resulting residue was lyophilised from water. The crude octapeptin A3 thus obtained was purified by RP-HPLC (Method 3). The final yield of octapeptin A3 as its TFA salt was 61.3 mg (45%, >97% purity). t_R 3.4 (Method 1). (ES) m/z 1032.8 ($M+Na^+$), 1010.7 (MH^+), 506.0 (MH_2^{2+}). HRMS exact mass (ESI microTOF-LC): calcd for $C_{48}H_{93}N_{13}O_{10}^+$ 505.8579 (MH_2^{2+}), found 505.8593. The overall yield of octapeptin A3 from H-L-Leu-2CT resin was 21%.

Bacterial strains and growth conditions—*P. aeruginosa* PAK*pmrB6* strain was obtained from Moskowitz Laboratory (Simches Research Center, Massachusetts General Hospital, Boston, MA). All bacteria were stored at -80°C in tryptone soya broth (Oxoid, Australia). Prior to experiments, parent strains were sub-cultured onto nutrient agar plates (Medium Preparation Unit, University of Melbourne, VIC, Australia). Overnight broth cultures were subsequently grown in 5 mL of cation-adjusted Mueller-Hinton broth

(CaMHB, Oxoid, Australia), from which a 1 in 100 dilution was performed in fresh broth to prepare mid-logarithmic cultures according to the optical density at 500 nm (OD_{500nm} = 0.4 to 0.6). All broth cultures were incubated at 37°C in a shaking water bath (180 rpm).

Minimum Inhibitory Concentration (MIC) microbiological assay—MICs for each strain were determined by the broth microdilution method.[24] Experiments were performed with CaMHB in 96-well polypropylene microtitre plates. Wells were inoculated with 100 μL of bacterial suspension prepared in CaMHB (containing 10^6 colony forming units (CFU) per mL) and 100 μL of CaMHB containing increasing concentrations of octapeptin A3 (0 to 256 mg/L). The MICs were defined as the lowest concentration at which visible growth was inhibited following 18 h incubation at 37°C. Cell viability was determined by sampling wells at polymyxin concentrations greater than the MIC. These samples were diluted in normal saline and spread plated onto nutrient agar. After incubation at 37°C for 20 h, viable colonies were counted on these plates. The limit of detection was 10 CFU/mL.

Mouse bacteremia model: All experiments performed were in accordance with the Australian code of practice for the care and use of animals for scientific purposes.25 All studies were approved by the Monash Institute of Pharmaceutical Sciences Animal Ethics Committee, Monash University (Parkville, Australia). Mice were housed in micro-isolated cages in a temperature (21 ± 3°) and humidity-controlled facility with a 12 h light-dark cycle (06:00-18:00) and acclimatized for 2 d. All animals received food and water *ad libutum*. The *in vivo* antibacterial activity of octapeptin A3 and the comparator polymyxin B was assessed against a panel of polymyxin-susceptible and -resistant clinical isolates of *P. aeruginosa* using our well established mouse blood infection model.26 The antibacterial activity of each lipopeptide was determined following a single intravenous dose (4 mg/kg) and the reduction in bacterial counts in blood was determined at 4 h.

Lipid A isolation and structural elucidation—Lipid A was isolated by mild acid hydrolysis.[27] In brief, the bacterial cells (OD_{600nm}= 0.8) from 1.5 L of liquid culture were harvested via centrifugation at 3,220 ×*g* for 30 min, and then washed twice with 50 mL of PBS. The cells were re-suspended in 40 mL of PBS, then chloroform (50 mL) and methanol (100 mL) were added to the suspension, producing a single-phase Bligh-Dyer mixture (chloroform/methanol/water, 1:2:0.8, v/v). [28] The mixture was centrifuged at 3,220×*g* for 15 min to remove the supernatant. The LPS pellet was washed once with 50 mL of chloroform/methanol/water (1:2:0.8, v/v) and re-suspended in 54 mL of hydrolysis buffer (50 mM sodium acetate pH 4.5, 1% sodium dodecyl sulfate [SDS]), and incubated in a boiling water bath for 45 min. To extract the lipids after hydrolysis, the SDS solution was converted into a double-phase Bligh-Dyer mixture by adding 60 mL of chloroform and 60 mL of methanol, forming a chloroform/methanol/water (1:1:0.9, v/v) mixture.[28] The lower phase containing lipid A was finally extracted. Samples were dried and purified using preparative thin-layer chromatography with multi-developing solvents system ($CHCl_3$/methanol//pyridine/acetic acid/H_2O, 10:5:4:3:2, v/v). Structural analysis of lipid A was performed by electrospray ionization (ESI) tandem mass spectrometry in negative mode performed on a Q-Exactive Hybrid Quandrupole-Orbitrap Mass Spectrometer (Thermo Fisher, Australia).

Displacement of the dansyl-polymyxin probe FADDI-043 from P. aeruginosa LPS—*P. aeruginosa* serotype 10 LPS suspensions (3 mg/L) were prepared in 5 mM HEPES buffer (pH 7.0). LPS was added into a quartz cuvette containing 1 mL of the same buffer, following which aliquots of FADDI-043 (aka MIPS-9541) solution were titrated at 2 min intervals until fluorescence intensity reached a plateau.[20-22] Fluorescence was measured using a Cary Eclipse fluorescence spectrophotometer (Varian, Mulgrave, Australia) set at an excitation wavelength of 340 nm. Slit widths were set to 5 and 10 nm for the excitation and emission monochromators, respectively. Emission spectrum was collected from a wavelength of 400 – 650 nm.

Fluorescence enhancement was determined from the integrated area under the emission spectrum. The dissociation constant (K_D) of the FADDI-043 complex with LPS was determined by non-linear regression analysis of the binding isotherms. The background-corrected FADDI-043 binding fluorescence data were fitted to a one-site binding model (Eq 1).

$$\Delta F = \Delta F_{max} * [L]/(K_D + [L]) \quad \text{(Eq 1)}$$

Where ΔF represents the specific fluorescence enhancement upon the addition of FADDI-043 to a fixed concentration of LPS or whole cells, ΔF_{max} is the maximum specific fluorescence enhancement at saturation, K_D represents the dissociation constant for FADDI-043 binding to LPS obtained from the concentration of FADDI-043 equivalent to half ΔF_{max} determined from the data fit, and [L] represents the total concentration of FADDI-043 (it is assumed that ligand depletion is not in effect and only a small fraction of the total FADDI-043 is bound).

For the displacement experiments, FADDI-043 (1.5 μM) was added to a quartz cuvette containing *P. aeruginosa* serotype 10 LPS at a concentration necessary to obtain 90 to 100% of the maximum fluorescence when bound. Displacement of FADDI-043 was measured as the corresponding decrease in fluorescence upon the progressive titration of aliquots of octapeptin A3 or colistin solutions at 2 min intervals, until no further decrease in fluorescence was observed.

Fluorescence readings were corrected for dilution before plotting the fraction of FADDI-043 bound as a function of the concentration of the displacing octapeptin A3 or colistin. The concentration of octapeptin A3 or colistin required to displace 50% of the bound FADDI-043 (I_{50}) was determined by fitting the fluorescence data to a sigmoidal dose-response model which assumed a single class of binding sites (Eq 2):

$$\%\,\text{Initial Fluorescence} = F_{min} + (F_{max} - F_{min})/(1 + 10^{((\log 150 - \log[L]) * \text{Hill Slope})}) \quad \text{(Eq 2)}$$

Where I_{50} is the midpoint of competition and is defined as the concentration of displacer at which the maximum fluorescence intensity (F_{max}) of the FADDI-043-saturated complex is reduced to 50% of the initial value; F_{min} represents the maximum FADDI-043 displacement produced by the competitor lipopeptide and is defined by the bottom plateau of the displacement curve; [L] represents the concentration of the competitor. The inhibition constant (K_i) is determined from the following equation (Eq 3):

$$K_i = [I_{50}]/(1 + [\text{FADDI} - 043]_{\text{free}}/K_{\text{D FADDI}-043}) \quad \text{(Eq 3)}$$

Where $K_{D\text{FADDI-043}}$ represents the dissociation constant for the FADDI-043 - LPS complex. All data modeling operations were performed with GraphPad Prism V5.0 software.

Isothermal Titration Calorimetry—Microcalorimetric experiments of octapeptin A3 and colistin binding to *P. aeruginosa* serotype 10 LPS were performed on a VP-ITC isothermal titration calorimeter (Microcal, Northampton, MA) at 37°C in 20 mM HEPES buffer (pH 7.0). The molar concentration of LPS was determined using the purpald Kdo assay.[29] All samples were thoroughly degassed beforehand. In the ITC experiments, *P. aeruginosa* serotype 10 LPS (0.125 mM) dissolved in 20 mM HEPES (pH 7.0) were filled into the microcalorimetric cell (volume, 1.3 mL) and titrated with 80 × 3 μL injections of a 3 mM octapeptin A3 or colistin solution at 240 s intervals from a 250 μL injection syringe. The cell contents were stirred constantly at 307 rpm. The system was allowed to equilibrate and a stable baseline was recorded before initiating an automated titration. The heat of interaction after each injection measured by the ITC instrument was plotted versus time. As a control for all ITC experiments, octapeptin A3 or colistin were titrated into buffer under the same injection conditions and the heat of dilution was subtracted from the LPS titration data. The total heat signal from each injection was determined as the area under the individual peaks and plotted versus the [lipopeptide]/[LPS] molar ratio.

The corrected data were analyzed to determine number of binding sites (n), and molar change in enthalpy of binding (ΔH) by nonlinear least square regression analysis in terms of an equation series that define two sets of independent sites.[30]

The binding constants (K) for each site are defined by Eq 4 & 5; Θ represents the fraction of sites occupied by the lipopeptide; and [X] is the free concentration of lipopeptide.

$$K1 = \frac{\Theta}{(1 - \Theta 1)[X]};\ K2 = \frac{\Theta}{(1 - \Theta 2)[X]} \quad \text{(Eq 4)}$$

The total concentration of lipopeptide X_t is defined by:

$$Xt = [X] + Mt(n1\Theta 1 + n2\Theta 2) \quad \text{(Eq 5)}$$

where M_t is the total concentration of LPS in V_o the active cell volume.

Solving Eq 5 for Θ1 and Θ2 and substituting into Eq 4 leads to the cubic equation of the form:

$$[X]^3 + p[X]^2 + q[X] + r = 0 \quad \text{(Eq 6)}$$

where

$$p = \frac{1}{K1} + \frac{1}{K2} + (n1 + n2)Mt - Xt$$

$$q = \left(\frac{n1}{K2} + \frac{n2}{K1}\right)Mt\left(\frac{1}{K1} + \frac{1}{K2}\right)Xt + \frac{1}{K1K2}$$

$$r = \frac{-Xt}{K1K2}$$

Eq 6 was solved for [X], then Θ1 and Θ2 were obtained from Eq 5.

Q the total heat content of the solution in V_o at fractional saturation Θ is given by:

$$Q = MtVo(n1\Theta 1\Delta H1 + n2\Theta 2\Delta H2) \quad \text{(Eq 7)}$$

Following correction for the displaced volume, the calculated heat effect from the *i*th injection is given by Eq 8 to obtain the best fit for *n1, n1*, K1, K2 and ΔH1, ΔH2 by standard Marquardt methods until no further significant improvement in fit occurs with continued iteration.[30-31]

$$\Delta Q(i) = Q(i) + \frac{dVi}{Vo}\left[\frac{Q(i) + Q(i-1)}{2}\right] - Q(i-1) \quad \text{(Eq 8)}$$

All data fitting operations were performed with Origin V8.0 (OriginLab, Northampton, MA).

ΔG^0 and ΔS^0 were calculated from the fundamental equations of thermodynamics Eq 9 and 10, respectively:

$$\Delta G^0 = -RTIn Ka \quad \text{(Eq 9)}$$

$$\Delta S^0 = (\Delta H - \Delta G^0)/T \quad \text{(Eq 10)}$$

Large unilaminar vesicle (LUV) dye-release assay—For LUV preparation, a phospholipid mixture was prepared to reflect the OM lipid composition of *P. aeruginosa* with a ratio of 7:3 palmitoyloleoyl-phosphatidylethanolamine (POPE): phosphatidylglycerol (POPG).[32] LUVs with LPS were prepared with the same phospholipid mixture composition POPE:POPG (7:3); where *P. aeruginosa* serotype 10 LPS was added accordingly to 1:1 v/v ratio to the lipid powders. The LUVS were then prepared as described above. The phospholipids were co- solubilized in chloroform/methanol (3:1 v/v) followed by removal of organic solvents by rotary evaporation. Lipid films were then hydrated with Milli-Q water to ensure homogeneity and lyophilized over-night. The resultant lipid film was re-suspended in 20 mM Tris-HCl buffer (pH 7.4), 100 mM NaCl and 80 mM calcein and subjected to three freeze-thaw cycles. The homogenous dispersions were extruded 21 times through an Avanti Mini-Extruder (Alabaster, AL) using a 0.2 μM polycarbonate filters to produce LUVs of ~200 nm in diameter. The LUV encapsulated dye was separated from the free dye using Sephadex G-100 gel filtration. The gel media and running buffer were degassed before use to prevent air bubbles forming in the column, which would inhibit separation of LUVs and free dye. Samples were eluted under gravity with 20 mM Tris-HCl buffer (pH 7.4), 100 mM NaCl as the running buffer at ~1 mL/min. The running buffer volume above the column bed height was held relatively constant by matching the elution flow rate with that of the buffer added to the top of the column. Fractions of 1 mL of dye-loaded LUVs were collected and pooled. Phospholipid concentrations were determined in triplicate using the phosphorus assay of Anderson *et al.*[33] The hydrodynamic radii of the extruded LUVs were measured on a Malvern Zetasizer NanoZS (Worcestershire, UK) at 25°C using a polystyrene sizing cuvette with 10 mm path-length.

Kinetic measurements of LUV calcein-release following lipopeptide treatment were performed on a Varian Cary Eclipse spectrophotometer (Mulgrave, Australia) at 25°C using a 10 mm path-length semi-micro quartz cell. The excitation wavelength was 490 nm and fixed wavelength fluorescence emission intensity was recorded at 515 nm. PMT voltage were set at low and emission was recorded every 20 s. Triton X-100 (2.5%) was employed as the positive control to achieve full release of calcein from LUVs. Calcein-release is measured as the increase in fluorescence intensity when the membrane is breached and the encapsulated dye is released into the external solution. The extent of calcein release was calculated according to Eq 11.

$$\%\,\text{dye} - \text{release} = \frac{(I - I^0)}{Imax - I^0} \times 100 \quad \text{(Eq 11)}$$

Where *I:* is the fluorescence intensity of lipopeptide treated LUV, *I°* is the intensity of the untreated LUV and *Imax* is the fluorescence intensity of the Triton X-100 treated supernatant (positive control).

Gram negative bacterial outer membrane model deposition—Deposition of the Gram-negative outer membrane models on single silicon crystal surfaces used a purpose-built Langmuir-Blodgett (LB) trough (Nima Technology, Coventry, UK). The cleaned trough was filled with 5 mM $CaCl_2$ solution and cooled to 10°C. The air-liquid interface was aspirated until clean and a silicon crystal block was submerged in the trough. The OM models were deposited onto the silicon surface using LB deposition for the deuterated dipalmitoylphosphatidylcholine (d62-DPPC) inner layer and followed by deposition of the lipid A outer layer via Langmuir Schaefer (LS) method (Figure S5). For the LB deposition of the inner bilayer leaflet, d62-DPPC was deposited from a 1 mg/mL solution in chloroform onto a clean air/liquid interface and compressed to a surface pressure of 35 mN/m. The submerged silicon crystal was lifted through the air-liquid surface at a speed of 6 mm/min with a constant air-liquid surface pressure. The LB trough was then cleaned and refilled with 5 mM $CaCl_2$ at 10°C. Ara4N-lipid A suspension at 2 mg/mL in chloroform:methanol:water solution (60:39:1 [v/v]) was then deposited onto the air/liquid interface and the surface pressure was compressed to 35 mM/m. The silicon crystal containing LB deposited d62-DPPC monolayer was fitted in a holder directly above the air/liquid interface of the LB trough. The angle of crystal was adjusted using a purpose-built levelling device to make the crystal surface parallel to the water surface. The silicon crystal with LB film was then dipped through the interface at a constant speed of 6 mm/min and lowered into a purpose-built sample cell in the well of the trough.

Neutron reflectometry measurements—NR measurements of the OM models were undertaken on the Platypus time-of-flight reflectometer and a cold neutron spectrum (2.8 Å $\leq \lambda \leq$ 18 Å) at the OPAL 20 MW research reactor (Sydney, Australia). The reflected intensity was measured at two glancing angles of 0.45° for 15 min and 1.6° for 60 min as a function of the momentum transfer, Qz ($Qz=[4\pi \sin \theta]/\lambda$, where λ is the wavelength and θ is the incident angle). Purpose-built liquid flow cells for analysis of the interface were placed on a variable angle sample stage in the NR instrument and the inlet to the liquid cell was connected to a liquid chromatography pump (L7100 HPLC pump, Merck, Hitachi); which allowed for easy exchange of the solution isotopic contrast (5 mL volume) within the solid-liquid sample cell. The bilayer structure was analysed in three solution isotopic contrasts (i) 100% D_2O, (ii) 38% D_2O and 62% of H_2O (which has the same neutron scattering length density (nSLD) as silicon surface, and thus called silicon-matched water, SMW), and (iii) 100% H_2O. For each change of the isotopic contrast solution, a total of 5 mL of 10 mM pH 7.4 HEPES buffer combined with 5 mM $CaCl_2$ and 150 mM NaCl solution was pumped through the cell at a speed of 1 mL/min. For the interaction of lipopeptides with the model OM bilayers, polymyxin B and octapeptin A3 were dissolved in 20 mM HEPES pH 7.4, 5 mM $CaCl_2$, 150 mM NaCl buffer solutions in D_2O which were then injected into the sample cells.

Neutron reflectometry data analysis—NR data was analysed using the MOTOFIT reflectometry analysis software. A least squares fitting routine selects the best fit by minimising &chi^2 values through varying the thickness, interfacial roughness and neutron scattering length density (nSLD) of each layer. In this approach the interface is described as a series of slabs, each of which is characterised by its nSLD, thickness and roughness. The reflectometry for the model starting point is then calculated and compared with the experimental data. In all cases, the model which contains the least number of layers was selected to adequately describe the data. In this study, the systems for NR data were asymmetrically deposited bilayers (i.e., d62-DPPC [inner layer]: Ara4N-lipid A [outer layer]). Each bilayer was examined under three isotopic contrast (D_2O, SMW, and H_2O) to yield three reflectometry profiles for each structure. A single profile of layer thickness and roughness were fitted for the three reflectometry profiles in the silicon deposited bilayer, but the SLD of each individual layer was allowed to vary in order to account for volume fraction. The parameter fit values and the SLD profiles described above were then used to determine the bilayer structure across and the surface coverage. The SLD of the tail regions of d62-DPPC labelled bilayer was used to determine lipid asymmetry.

The volume fractions of Ara4N-lipid A and DPPC in the head group layers could be ascertained due to the minimal isotopic contrast between the Ara4N-lipid A GlcN head groups and the DPPC head groups. The total amount of Ara4N-lipid A and DPPC head groups could be estimated by determining the volume fraction of water in the inner and outer head group regions and comparing the fitted SLDs of the differing solution contrasts to the known SLD of H_2O and D_2O.

The SLDs of polymyxin B and octpeptin A3 were calculated using SL calculator and changes in the SLD due to labile hydrogen exchange with D_2O, SMW and H_2O. The coverage of lipopeptides in their binding layers was determined by comparing the fitted SLD values of these layers to the calculated SLD values of lipopeptides, lipids, and water (Table S7).[17-19]

Supplementary Material

Refer to Web version on PubMed Central for supplementary material.

Acknowledgments

J.L. and T.V. are supported by research grants from the National Institute of Allergy and Infectious Diseases of the National Institutes of Health (R01A1070896 and R01AI079330). J.L., T.V. H.H.S. and M.A.C. are also supported by the Australian National Health and Medical Research Council (NHMRC). The content is solely the responsibility of the authors and does not necessarily represent the official views of the National Institute of Allergy and Infectious Diseases or the National Institutes of Health.

References

1. Bratu S, Tolaney P, Karumudi U, Quale J, Mooty M, Nichani S, Landman D. Carbapenemase-producing *Klebsiella pneumoniae* in Brooklyn, NY: molecular epidemiology and in vitro activity of polymyxin B and other agents. J Antimicrob Chemother. 2005; 56(1):128–32. doi:dki175 [pii]10.1093/jac/dki175[doi]. [PubMed: 15917285]

2. Elemam A, Rahimian J, Mandell W. Infection with panresistant Klebsiella pneumoniae: a report of 2 cases and a brief review of the literature. Clin Infect Dis. 2009; 49(2):271–4. DOI: 10.1086/600042[doi] [PubMed: 19527172]

3. Kato T, Shoji T. The structure of octapeptin D (studies on antibiotics from the genus Bacillus. XXVIII). J Antibiot (Tokyo). 1980; 33(2):186–91. [PubMed: 7380727]

4. Konishi M, Sugawara K, Tomita K, Matsumoto K, Miyaki T, Fujisawa K, Tsukiura H, Kawaguchi H. Bu-2470, a new peptide antibiotic complex. I. Production, isolation and properties of Bu-2470 A, B1 and B2. J Antibiot (Tokyo). 1983; 36(6):625–33. [PubMed: 6874583]

5. Meyers E, Brown WE, Principe PA, Rathnum ML, Parker WL. EM49, a new peptide antibiotic. I. Fermentation, isolation, and preliminary characterization. J Antibiot (Tokyo). 1973; 26(8):444–8. [PubMed: 4209531]

6. Shoji J, Hinoo H, Wakisaka Y, Koizumi K, Mayama M. Isolation of a new antibiotic 333-25, related to antibiotic EM 49. (Studies on antibiotics from the genus Bacillus. XI). J Antibiot (Tokyo). 1976; 29(5):516–20. [PubMed: 956039]

7. Sugawara K, Yonemoto T, Konishi M, Matsumoto K, Miyaki T, Kawaguchi H. Bu-2470, a new peptide antibiotic complex. II. Structure determination of Bu-2470 A, B1, B2a and B2b. J Antibiot (Tokyo). 1983; 36(6):634–8. [PubMed: 6874584]

8. Meyers E, Parker WL, Brown WE. A nomenclature proposal for the octapeptin antibiotics. J Antibiot (Tokyo). 1976; 29(11):1241–2. [PubMed: 993110]

9. Meyers E, Parker WL, Brown WE, Linnett P, Strominger JL. EM49: a new polypeptide antibiotic active against cell membranes. Ann N Y Acad Sci. 1974; 235(0):493–501. [PubMed: 4368713]

10. Parker WL, Rathnum ML. EM49, a new peptide antibiotic IV. The structure of EM49. J Antibiot (Tokyo). 1975; 28(5):379–89. [PubMed: 170240]

11. Shoji J, Hinoo H, Sakazaki R. The constituent amino acids and fatty acid of antibiotic 333-25. (Studies on antibiotics from the genus Bacillus. XII. J Antibiot (Tokyo). 1976; 29(5):521–5. [PubMed: 956040]

12. Storm DR, Rosenthal KS, Swanson PE. Polymyxin and related peptide antibiotics. Annu Rev Biochem. 1977; 46:723–63. DOI: 10.1146/annurev.bi.46.070177.003451 [PubMed: 197881]

13. Parker WL, Rathnum ML. EM49, a new peptide antibiotic. II. Chemical characterization. J Antibiot (Tokyo). 1973; 26(8):449–56. [PubMed: 4792068]

14. Moskowitz SM, Ernst Rk, Fau - Miller SI, Miller SI. PmrAB, a two-component regulatory system of Pseudomonas aeruginosa that modulates resistance to cationic antimicrobial peptides and addition of aminoarabinose to lipid A. J Bacteriol. 2004; 186(2):575–579. doi:D - NLM: PMC305751 EDAT- 2004/01/02 05:00 MHDA- 2004/01/30 05:00 CRDT- 2004/01/02 05:00 PST - ppublish. [PubMed: 14702327]

15. Shen HH, Leyton DL, Shiota T, Belousoff MJ, Noinaj N, Lu J, Holt SA, Tan K, Selkrig J, Webb CT, Buchanan SK, Martin LL, Lithgow T. Reconstitution of a nanomachine driving the assembly of proteins into bacterial outer membranes. Nat Commun. 2014; 5:5078.doi: 10.1038/ncomms6078 [PubMed: 25341963]

16. Shen HH, Thomas RK, Chen CY, Darton RC, Baker SC, Penfold J. Aggregation of the naturally occurring lipopeptide, surfactin, at interfaces and in solution: an unusual type of surfactant? Langmuir. 2009; 25(7):4211–8. [PubMed: 19714837]

17. Clifton LA, Skoda MWA, Daulton EL, Hughes AV, Le Brun AP, Lakey JH, Holt SA. Asymmetric phospholipid: lipopolysaccharide bilayers; a Gram-negative bacterial outer membrane mimic. Journal of The Royal Society Interface. 2013; 10(89)doi: 10.1098/rsif.2013.0810

18. Clifton LA, Skoda MWA, Le Brun AP, Ciesielski F, Kuzmenko I, Holt SA, Lakey JH. Effect of Divalent Cation Removal on the Structure of Gram-Negative Bacterial Outer Membrane Models. Langmuir. 2015; 31(1):404–412. DOI: 10.1021/la504407v [PubMed: 25489959]

19. Clifton LA, Holt SA, Hughes AV, Daulton EL, Arunmanee W, Heinrich F, Khalid S, Jefferies D, Charlton TR, Webster JRP, Kinane CJ, Lakey JH. An Accurate In Vitro Model of the E. coli Envelope. Angewandte Chemie International Edition. 2015; 54(41):11952–11955. DOI: 10.1002/anie.201504287 [PubMed: 26331292]

20. Azad MA, Yun B, Roberts KD, Nation RL, Thompson PE, Velkov T, Li J. Measuring polymyxin uptake by renal tubular cells: is BODIPY-polymyxin B an appropriate probe? Antimicrobial agents

and chemotherapy. 2014; 58(10):6337–6338. doi:D - NLM: PMC4187948 EDAT- 2014/09/17 06:00 MHDA- 2015/09/12 06:00 CRDT- 2014/09/17 06:00 AID - 58/10/6337 [pii] AID - 10.1128/AAC.03733-14 [doi] PST - ppublish. [PubMed: 25225340]

21. Deris ZZ, Swarbrick JD, Roberts KD, Azad MAK, Akter J, Horne AS, Nation RL, Rogers KL, Thompson PE, Velkov T, Li J. Probing the Penetration of Antimicrobial Polymyxin Lipopeptides into Gram-Negative Bacteria. Bioconjugate Chemistry. 2014; 25(4):750–760. DOI: 10.1021/bc500094d [PubMed: 24635310]
22. Yun B, Azad MA, Nowell CJ, Nation RL, Thompson PE, Roberts KD, Velkov T, Li J. Cellular Uptake and Localization of Polymyxins in Renal Tubular Cells Using Rationally Designed Fluorescent Probes. Antimicrobial Agents and ChemotherPY. 2015; 59(12):7489–7496. doi:D - NLM: PMC4649194 EDAT- 2015/09/24 06:00 MHDA- 2016/09/01 06:00 CRDT- 2015/09/23 06:00 PHST- 2015/05/28 [received] PHST- 2015/09/14 [accepted] AID - AAC.01216-15 [pii] AID - 10.1128/AAC.01216-15 [doi] PST - ppublish.
23. Sani MA, Gagne E, Gehman JD, Whitwell TC, Separovic F. Dye-release assay for investigation of antimicrobial peptide activity in a competitive lipid environment. European Biophysics Journal. 2014; 43(8):445–450. DOI: 10.1007/s00249-014-0970-0 [PubMed: 24906225]
24. Wiegand I, Hilpert K, Hancock RE. Agar and broth dilution methods to determine the minimal inhibitory concentration (MIC) of antimicrobial substances. Nat Protoc. 2008; 3(2):163–75. doi:nprot.2007.521 [pii] 10.1038/nprot.2007.521 [doi]. [PubMed: 18274517]
25. Australia, N. H. a. M. R. C. o. Australian code of practice for the care and use of animals for scientific purposes 8th edition. 2014
26. Dudhani, RV., Li, J., Turnidge, JD., Coulthard, K., Milne, RW., Rayner, CR., Nation, RL. Pharmacokinetics/Pharmacodynamics of colistin sulfate against Pseudomonas aeruginosa ATCC 27853 in murine thigh and lung infection models. 47th Annual Interscience Conference on Antimicrobial Agents and Chemotherapy (ICAAC), Chicago; September 16 to 19; American Society for Microbiology: Chicago. 2007.
27. Que NL, Lin S, Cotter RJ, Raetz CR. Purification and Mass Spectrometry of Six Lipid A Species from the Bacterial Endosymbiont Rhizobium etli DEMONSTRATION OF A CONSERVED DISTAL UNIT AND A VARIABLE PROXIMAL PORTION. Journal of Biological Chemistry. 2000; 275(36):28006–28016. [PubMed: 10856303]
28. Bligh EG, Dyer WJ. A rapid method of total lipid extraction and purification. Canadian journal of biochemistry and physiology. 1959; 37(8):911–917. [PubMed: 13671378]
29. Lee CH, Tsai CM. Quantification of bacterial lipopolysaccharides by the purpald assay: measuring formaldehyde generated from 2-keto-3-deoxyoctonate and heptose at the inner core by periodate oxidation. Anal Biochem. 1999; 267(1):161–8. doi:S0003-2697(98)92961-X [pii] 10.1006/abio.1998.2961. [PubMed: 9918668]
30. Origin, Origin 8 User Guide. Northampton, MA: 2007. OriginLab Corporation. http://www.llas.ac.cn/upload/Origin_8_User_Guide.pdf
31. Marquardt D. An algorithm for least-squares estimation of nonlinear parameters. SIAM J Appl Math. 1963; 11:431–441.
32. Sani MA, Gagne E, Fau - Gehman JD, Gehman Jd, Fau - Whitwell TC, Whitwell Tc, Fau - Separovic F, Separovic F. Dye-release assay for investigation of antimicrobial peptide activity in a competitive lipid environment. Eur Biophys J. 2014; 43(809):445–450. [PubMed: 24906225]
33. Anderson RL, Davis S. An organic phosphorus assay which avoids the use of hazardous perchloric acid. Clin Chim Acta. 1982; 121(1):111–6. [PubMed: 6282500]

Synopsis

The paper covers the first in toto synthesis, mode of action, and in vivo efficacy of a class of octapeptin A3, an example of the octapeptin cyclic lipopeptides that was first reported in the 1970s, then forgotten. As shown in our manuscript, octapeptin A3 displays significant antibacterial activity against XDR Gram-negative pathogens, including those resistant to polymyxins. This research is of high general interest due to the importance of developing new therapies for highly drug resistant bacterial infections, as recognised by multiple recent government strategy papers and strategic initiatives.

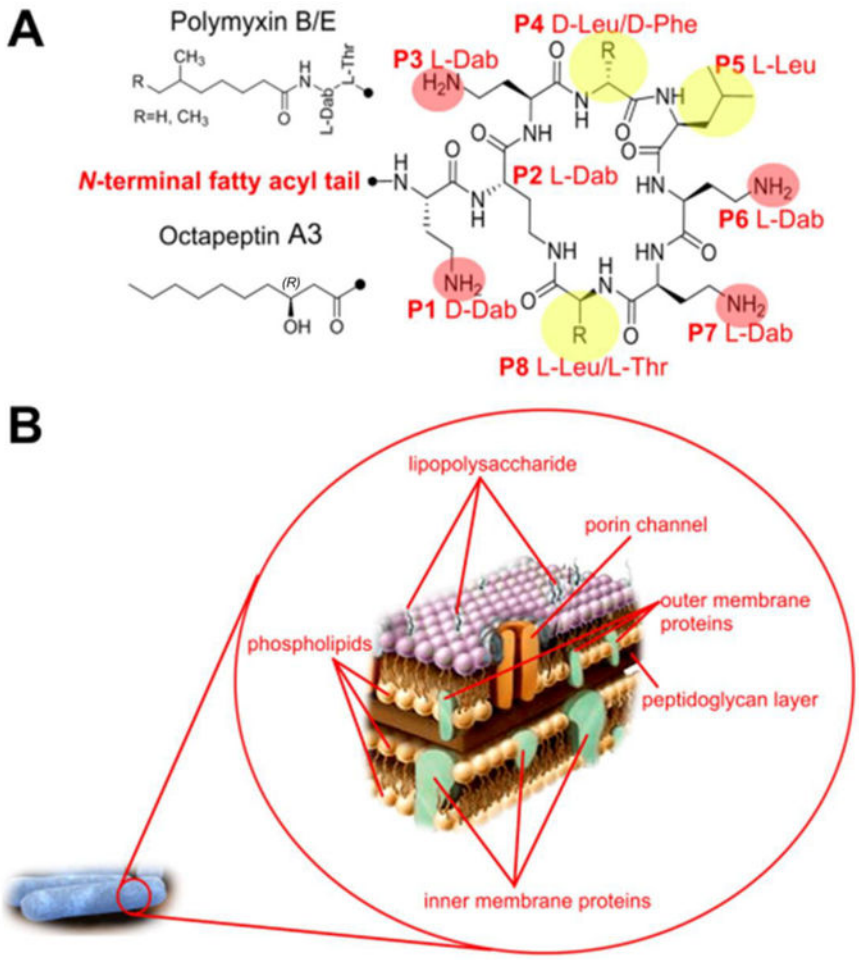

Figure 1.

(**A**) Chemical structures of polymyxin B and octapeptin A3. Leu: leucine; Phe: phenylalanine; Dab: α,γ-diaminobutyric acid. The hydrophobic side-chains are shaded yellow and the hydrophilic side-chains are shaded red; and (**B**) Schematic representation of the Gram-negative cell envelope.

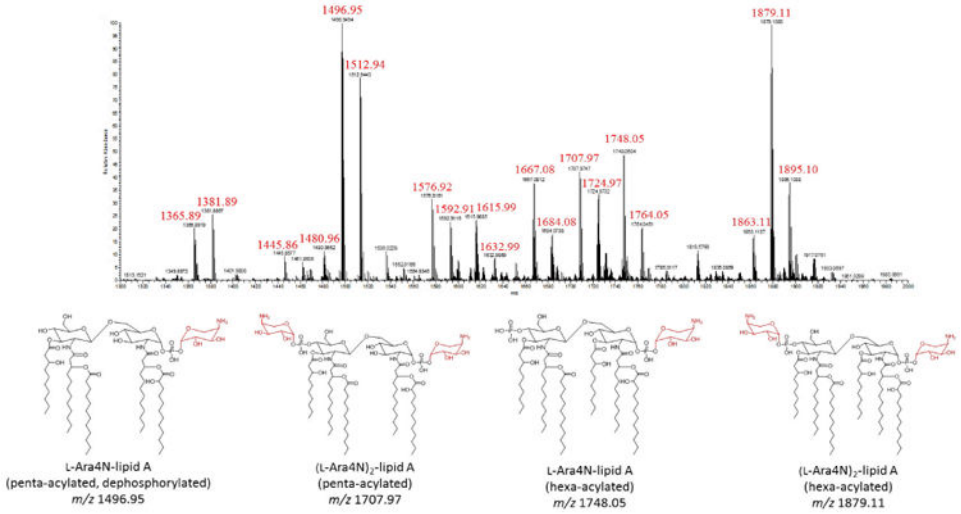

Figure 2.

MS profile and typical structures of lipid A isolated from the polymyxin-resistant *P. aeruginosa* strain PAK*pmrB6*. The mass spectrum was collected in negative ion mode.

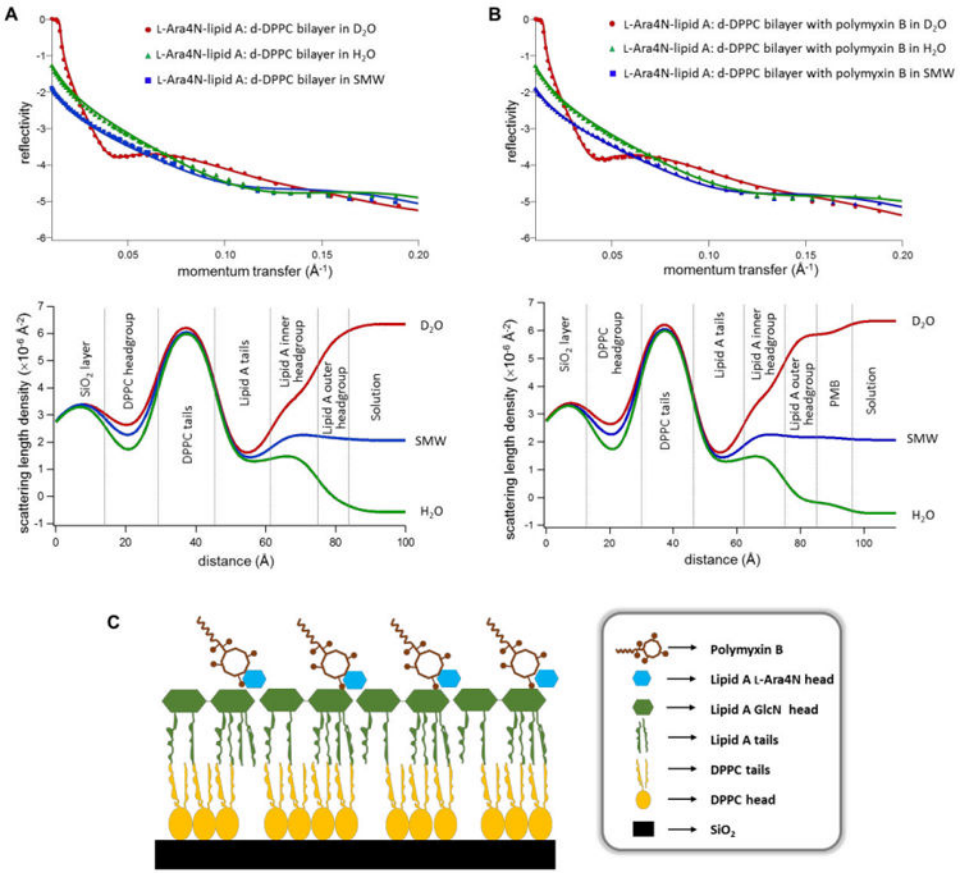

Figure 3.

(**A**) Neutron reflectometry profiles, calculated fits and the scattering length density profiles for the L-Ara4N modified lipid A : d-DPPC bilayer system; (B) the bilayer bound with polymyxin B at 4 mg/L in different water contrasts; (C) Schematic representation of the interfacial structure of Ara4N-lipid A : d62-DPPC bilayer binding with 4 mg/L polymyxin B. SMW: silicon matched water, which contains 38% D_2O and 62% H_2O.

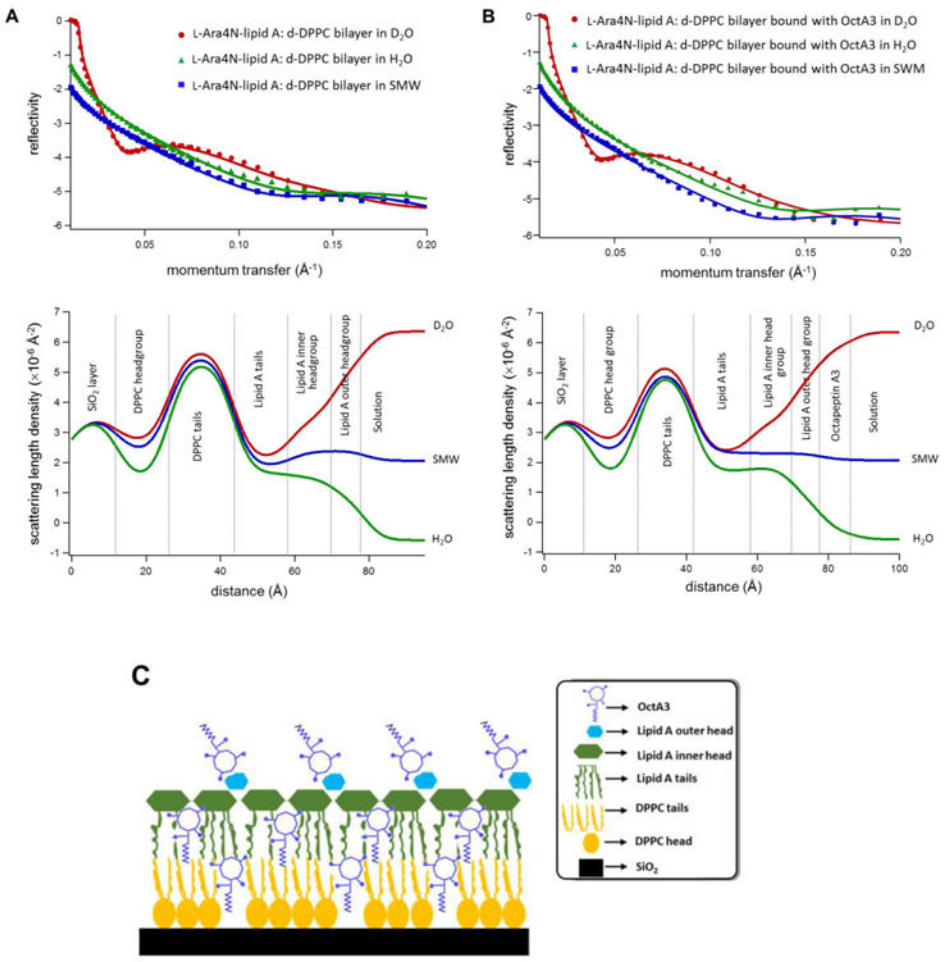

Figure 4.

(**A**) Neutron reflectometry profiles, calculated fits and the scattering length density profiles for the L-Ara4N modified lipid A : d62-DPPC bilayer system, and (**B**) the bilayer bound with octapeptin A3 at 1 mg/L in different water contrasts. (**C**) Schematic representation of the interfacial structures of Ara4N-lipid A : d62-DPPC bilayer after the addition of 1 mg/L octapeptin A3 (OctA3). SMW: silicon matched water, which contains 38% D_2O and 62% H_2O.

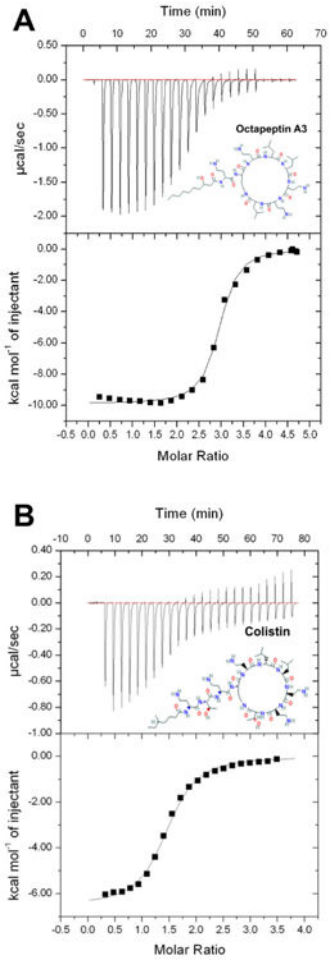

Figure 5.

ITC measurement of (A) octapeptin A3, and (B) colistin binding to *P. aeruginosa* serotype 10 LPS at 37°C in 20 mM HEPES buffer (pH 7.0). The thermodynamic parameters (enthalpy (ΔH), entropy (ΔS) and free energy (ΔG)) derived from the binding isotherms, together with the stoichiometry and binding affinity constants are documented in Table S3.

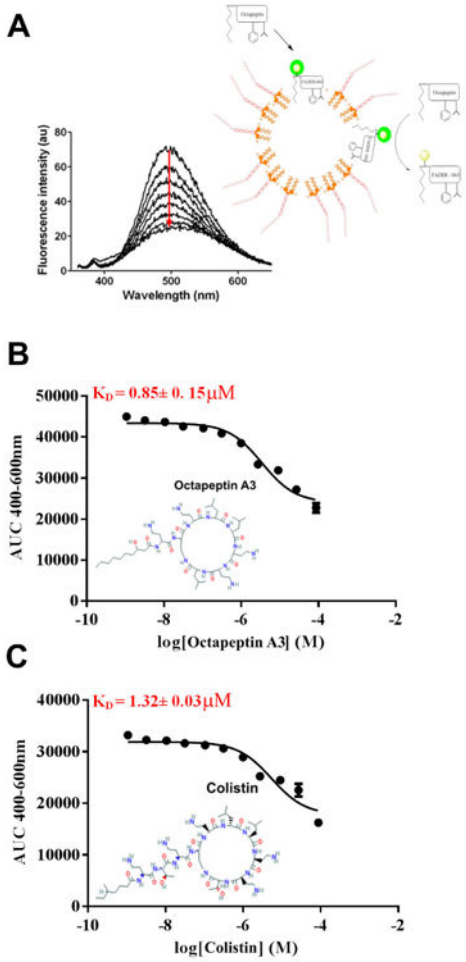

Figure 6.

(**A**) Raw fluorometric data for the displacement of the fluorescent dasnyl-polymyxin B probe (FADDI-043) from *P. aeruginosa* serotype 10 LPS micelles by octapeptin A3; and (**B**) the corresponding decrease in FADDI-043 fluorescence emission plotted as a function of the octapeptin A3 concentration. (**C**) colistin displacement data. Solid lines represent non-linear least squares regression fit of the data to a one site displacement model and the derived binding affinity constants are shown in red text.

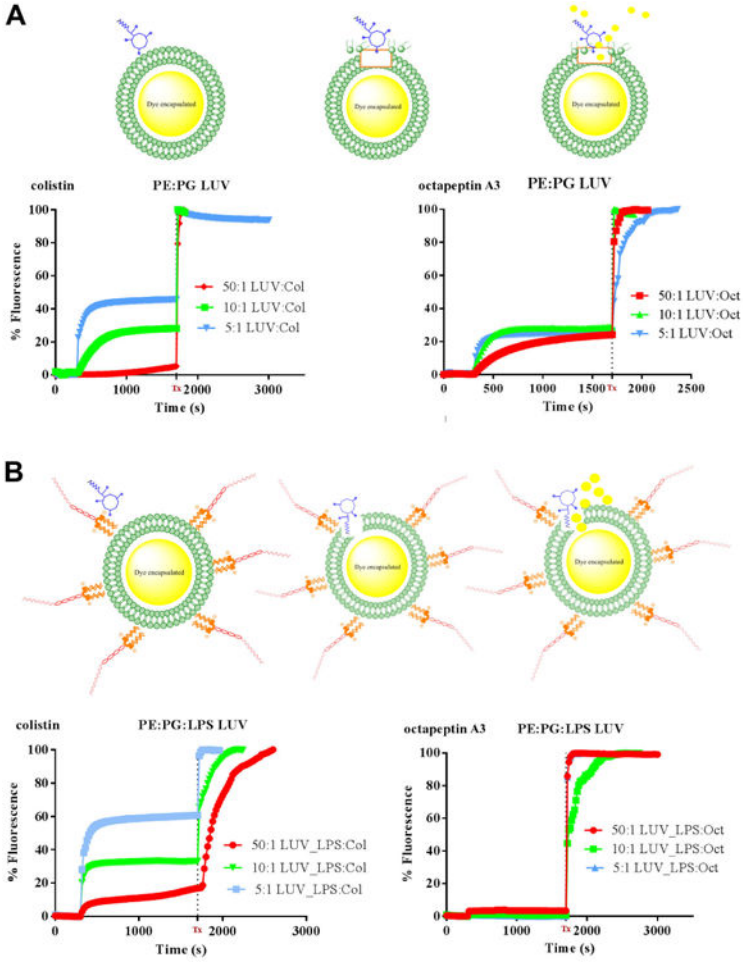

Figure 7.

Octapeptin A3 and colistin induced carboxyfluorescein dye release from (A) PE:PG large unilamellar vesicles (LUVs) and (**B**) PE:PG LUVs loaded with *P. aeruginosa* LPS. Emission was recorded at 515 nm every 20 sec. The fluorescence intensity is normalised to represent the percentage of maximum fluorescence intensity, achieved with the addition of Triton X-100 (dotted line, Tx).

ACS Infect Dis. Author manuscript; available in PMC 2018 May 16.

Table 1

Thicknesses and volume fractions of each layer in the asymmetric Ara4N-lipid A: d-DPPC bilayer system with an absorption of polymyxin B at 4 mg/L.

Layer[a]	Thickness (Å)	% DPPC	% Lipid A	% Water	%Polymyxin B
SiO_2	14.7±3.1	NA[b]	NA[b]	5	NF[d]
DPPC inner head	14.2±1.2	89.8[c]		10.2	NF[d]
DPPC inner tail	17.0±2.7	83	13.5	3.5	NF[d]
Lipid A outer tail	15.9±2.6	20.4	76.8	2.8	NF
Lipid A GlcN head	12.7±1.2	91.3[c]		8.7	NF[d]
Lipid A Ara4N head	9.0±0.5	NA[b]	64.8	35.2	NF[d]
polymyxin B (4 mg/L)	10.0±0.4	NA[b]	NA[b]	78.3±1.3	21.7±1.3

[a] Roughness of each layer was fitted at 4.0 ± 1.0 Å

[b] NA: not available

[c] Total volume fraction of lipid A and DPPC head groups within the fitted layer, which was determined according to the minimal isotopic contrast between the head groups of lipid A and DPPC, while bilayer asymmetry was calculated according to the neutron scattering length densities (nSLDs) of the tail regions of lipid A and d-DPPC in three isotopic contrast (D_2O, SMW and H_2O)

[d] NF: not found.

Table 2

Structural parameters and volume fractions for the asymmetric Ara4N-lipid A: DPPC bilayer system used for the octapeptin A3 interaction NR studies.

Layer[a]	Thickness (Å)	% DPPC	% Lipid A	% Water
SiO_2	12.0±1.9	NA[b]	NA[b]	5
DPPC inner head	14.0±1.0	88.6[c]		11.4
DPPC inner tail	17.2±0.2	73.5	21.6	4.9
Lipid A outer tail	15.8±3.2	26.5	67.4	6.1
Lipid A GlcN head	11.2±0.9	87.1[a]		12.9
Lipid A Ara4N head	8.5±0.5	NA	44.8	55.2

[a] Roughness of each layer was fitted at 4.0 ± 1.0 Å

[b] NA: not available

[c] Total volume fraction of lipid A and DPPC head groups within the fitted layer, which was determined according to the minimal isotopic contrast between the head groups of lipid A and DPPC, while bilayer asymmetry was calculated according to the neutron scattering length densities (nSLDs) of the tail regions of lipid A and d-DPPC in three isotopic contrast (D_2O, SMW and H_2O).

Table 3

Thicknesses and volume fractions of each layer in the asymmetric Ara4N-lipid A: d-DPPC bilayer system with an absorption of octapeptin A3 at 1 mg/L.

Layer[a]	Thickness (Å)	% DPPC	% Lipid A	% Water	%Octapeptin A3
SiO_2	12.2±2.0	NA[b]	NA[b]	5	NF[d]
DPPC inner head	14.0±1.9	88.6[c]		11.4	NF[d]
DPPC inner tail	15.6±0.5	62.7	18.4	0	17.3±1.6
Lipid A outer tail	16.6±4.6	20.9	53.3	0	25.8±2.5
Lipid A GlcN head	11.5±1.5	87.1[b]		7.4	5.5±2.0
Lipid A Ara4N head	7.9±0.8	NA[b]	44.8	45.9	9.3±1.4
Octapeptin A3 (1 mg/L)	9.6±0.6	NA[b]	NA[b]	83.9	16.1±0.5

[a] Roughness of each layer was fitted at 4.0 ± 1.0 Å.

[b] NA: not available.

[c] Total volume fraction of lipid A and DPPC head groups within the fitted layer, which was determined according to the minimal isotopic contrast between the head groups of lipid A and DPPC, while bilayer asymmetry was calculated according to the neutron scattering length densities (nSLDs) of the tail regions of lipid A and d-DPPC in three isotopic contrast (D_2O, SMW and H_2O).

[d] NF: not found.